An exact polyhedral model for boron nanotubes

2009 J. Phys. A: Math. Theor. 42 065204

(http://iopscience.iop.org/1751-8121/42/6/065204)

IOP PUBLISHING JOURNAL OF PHYSICS A: MATHEMATICAL AND THEORETICAL

J. Phys. A: Math. Theor. **42** (2009) 065204 (23pp) doi:10.1088/1751-8113/42/6/065204

An exact polyhedral model for boron nanotubes

Richard K F Lee, Barry J Cox and James M Hill

Nanomechanics Group, School of Mathematics and Applied Statistics, University of Wollongong, Wollongong, NSW 2522, Australia

E-mail: barryc@uow.edu.au

Received 19 August 2008, in final form 3 December 2008
Published 14 January 2009
Online at stacks.iop.org/JPhysA/42/065204

Abstract

An exact idealized polyhedral model is formulated to describe the geometry of single-walled boron nanotubes. The boron nanotubes considered here are assumed to be formed by sp^2 hybridization and adopt a flat equilateral triangle pattern. Beginning from the two fundamental postulates that all bond lengths are equal and all atoms are equidistant from a common cylindrical axis, we derive exact formulae for the geometric parameters of the nanotube radius, bond angle and unit cell length, and we present asymptotic expansions for these quantities to the first two orders of magnitude. Good agreement is demonstrated for the predictions of the polyhedral model, compared with the results obtained from first-principles simulations. The polyhedral model allows the possible identification of an inner radius, so that the notion of nanotube wall thickness can be introduced. Finally, we examine the geometric structure of some ultra-small boron nanotubes.

PACS numbers: 61.46.Np, 61.46.Fg, 61.46.−w

(Some figures in this article are in colour only in the electronic version)

1. Introduction

In the periodic table, boron is a neighbour of carbon and its chemical richness is second only to carbon due to its three valence electrons. Since carbon nanotubes were discovered by Iijima in 1991 [1], there have been many theoretical and experimental investigations of their properties, such as their large axial Young's modulus and high mechanical strength [2, 3]. This has triggered interest in other materials which may also exhibit such extreme properties. Due to its similarity and its rich chemistry, boron is a natural choice for constructing nanostructures, such as clusters, nanowires and nanotubes. Boron nanowires were discovered in 2002 [4, 5] and single-walled pure boron nanotubes were synthesized in 2004 [6–10].

Boron and carbon independently have very stable structures formed from sp^2 hybridized bonds [8, 11–17], but they have a different lattice structure. Carbon nanotubes are constructed

from a hexagonal honeycomb lattice [1], while a number of lattice structures have been proposed for boron nanotubes including flat equilateral triangles [8, 12, 13, 18–23] and puckered equilateral triangles [9, 14, 15, 20, 21, 24–26]. Recently, a novel lattice pattern is proposed comprising flat equilateral triangles mixed with hexagons, which is found to be more stable than the other lattice patterns for boron nanotubes [27]. However, although this configuration is thought to be more stable, an examination of the actual numerical data determined by these authors reveals that their model possesses three distinct radii [27, 28], and perhaps this internal and external 'puckering' arises as a consequence of the mixed lattice structure assumption. We further comment that even more exotic lattice patterns are proposed in [16]. Here for simplicity we consider the lattice for boron nanotubes to comprise only equilateral triangles with vertices that are all equidistant from a common axis.

Previous work on the structure of boron nanotubes assume the conventional 'rolled-up' model [18, 23], which is entirely analogous to the 'rolled-up' model for carbon nanotubes [29–31]. Recently, Cox and Hill [32, 33] have proposed a new polyhedral model for single-walled carbon nanotubes and the geometric parameters predicted by the polyhedral model are in excellent agreement with first-principles calculations [32]. In the present work, we employ a similar polyhedral model to represent single-walled boron nanotubes. For simplicity we assume that the lattice of the boron sheet employed here consists of only equilateral triangles. Although a hexagonal pattern [16, 27] with an extra atom at the centre of two-thirds of the hexagons is thought to be more stable, as mentioned above, the detailed numerical data of this model [28] possess three distinct radii and therefore it is not amenable as a simple polyhedral model. We comment that in proposing the new polyhedral model having all bond lengths equal, we have in mind a first level idealized model, for which any subsequent modifications such as unequal bond lengths can be incorporated later into the ideal model and the effect may be viewed as deviations from the ideal model behaviour.

The traditional model for carbon nanotubes is the 'rolled-up' formulation [29–31], in which it is assumed that a flat sheet of graphene is rolled into a right circular cylinder. Carbon nanotubes are categorized into three types namely armchair, zigzag and chiral, based on the values of the chiral vector numbers (n, m). The conventional model for boron nanotubes also follows this approach, and the lattice for the conventional boron nanotubes comprises a flat equilateral triangular pattern [18, 23]. The naming convention for boron nanotubes follows Gindulyte *et al* [18], that is exactly the same as for carbon nanotubes. Therefore, boron nanotubes are termed 'zigzag' when $m = 0$ and 'armchair' when $m = n$. In all other cases, when $0 < m < n$ they are termed 'chiral' nanotubes.

Employing the same approach as that used for the new polyhedral model for carbon nanotubes [32, 33], a polyhedral model for boron nanotubes is developed, which is based on two fundamental postulates: (i) all bond lengths are equal to the bond length σ and (ii) all atomic nuclei are equidistant a distance r from a common axis. Boron nanotubes as represented by the polyhedral model are shown in figure 1, where the boron atoms are shown by black dots, and the bonds between boron atoms are indicated by lines. The number of fundamental postulates for boron nanotubes are fewer than is the case for carbon nanotubes because the adjacent bond angle $\phi = 60^\circ$ for the boron nanotubes may be derived immediately from postulate (i) trivially, and therefore an independent adjacent bond angle postulate is not required.

In the following section we introduce the polyhedral model for boron nanotubes and the derivations for the major physical parameters of the polyhedral model. In section 3, we give the asymptotic expansions for these formulae for the first two leading terms. In section 4, we explore the geometric structure of some ultra-small nanotubes and in section 5, we describe the general behaviour of the major geometric parameters. In section 5 we also compare our

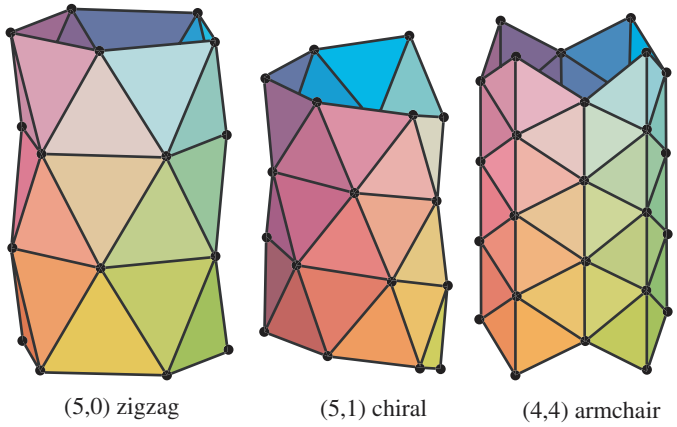

Figure 1. Boron nanotubes for polyhedral model for armchair, chiral and zigzag type.

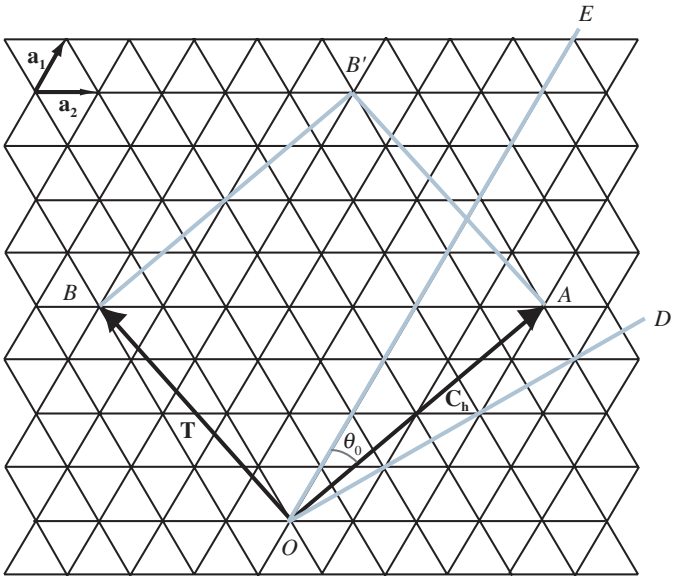

Figure 2. Boron nanotube constructed from two-dimensional sheet.

results and demonstrate good agreement with density functional theory or first-principles simulations. Some concluding remarks are made in section 6 and finally the details of the asymptotic expansions are presented in appendix A.

2. Polyhedral model for boron nanotubes

In the present work we follow the (n, m) naming scheme employed for boron nanotubes following Gindulyte *et al* [18]. The naming scheme identifies the specific configuration of the boron nanotube originating from the 'rolled-up' model, in which the boron nanotube is conceptualized as a flat plane of six-coordinated boron atoms, which is then rolled into a right circular cylinder. From figure 2, three different categories of boron nanotubes may be

defined, depending on the values of n and m. When $m = 0$, which is equivalent to rolling up the nanotubes in the direction of OE, the boron nanotubes are termed zigzag nanotubes. The second type occurs when $m = n$, which is equivalent to rolling the nanotubes in the direction of OD, and these tubes are termed armchair. If the direction of rolling lies between OD and OE, then the nanotubes are termed chiral. The direction of rolling of the nanotube is represented by the chiral vector $\mathbf{C_h}$ as shown in figure 2. In this figure, the example of a boron nanotube of type (4, 2) is depicted. The vector OB is called a unit translational vector $\mathbf{T}$ which is normalized by the greatest common divisor d_R of its components so that we have

$$\mathbf{C_h} = n\mathbf{a_1} + m\mathbf{a_2}, \qquad \mathbf{T} = (n + 2m)\mathbf{a_1}/d_R - (2n + m)\mathbf{a_2}/d_R,$$

where n and m are non-negative integer chiral vector numbers, $\mathbf{a_1}$ and $\mathbf{a_2}$ are the unit basis vectors in real space and d_R is the greatest common divisor of $n + 2m$ and $2n + m$. As shown in figure 2, the origin O is located at an arbitrary lattice point. The chiral vector $\mathbf{C_h}$ goes from O to A and the vector from O to B is called the translational vector $\mathbf{T}$. The sheet is rolled so that the point A coincides with the origin O and the point B coincides with the point B'.

The conventional chiral angle θ_0 as shown in figure 2 is defined as the angle between OE and OA and is given by

$$\cos\theta_0 = (2n + m)\Big/\left[2\sqrt{(n^2 + nm + m^2)}\right]. \tag{1}$$

The unit cell length L_0 for the rolled-up model is the length of the translational vector $|\mathbf{T}|$ and is given by

$$L_0 = \sigma\sqrt{3(n^2 + nm + m^2)}/d_R. \tag{2}$$

The conventional radius r_0 is given by the magnitude of the chiral vector $|\mathbf{C_h}|$ divided by 2π and thus

$$r_0 = \sigma\sqrt{n^2 + nm + m^2}/(2\pi). \tag{3}$$

The polyhedral model for boron nanotubes is similar to the corresponding carbon nanotube polyhedral model [32, 33]. For carbon nanotubes, each hexagonal face cannot be coplanar in the rolled-up state since all atoms in the carbon nanotube are equidistant from a common axis, thus elements of the hexagonal lattice are divided into three isosceles triangles and one equilateral triangle [32, 33]. However, the boron nanotubes lattice does not need to be subdivided because the triangular lattices are coplanar.

To derive the formulae for the polyhedral model, we begin by defining a cylinder upon which is traced helices that correspond to the lattice lines in the direction of $\mathbf{a_1}$. We can see from figure 2, that the number of helices is equivalent to the value of m, and all the boron atoms lie on these helices. To this end, we define a helix $\alpha(t)$ on the cylinder that in Cartesian coordinates is given parametrically by

$$\alpha(t) = (r\cos(2\psi t/m), r\sin(2\psi t/m), bt/m), \tag{4}$$

where 2ψ is the angle subtended at the nanotube axis in the xy-plane of one edge of a triangle, r is the nanotube radius, b is the helical vertical spacing coefficient and t is a parametric variable which has been chosen such that the vertices are spaced evenly by the distance m in this variable. Similarly, we define a second helix $\beta(t)$ is which congruent to $\alpha(t)$ but rotated through an angle of $2\pi/m$ thus it is given parametrically by

$$\beta(t) = (r\cos[2(\psi t - \pi)/m], r\sin[2(\psi t - \pi)/m], bt/m). \tag{5}$$

We also require a third helix $\gamma(t)$, which is congruent to $\beta(t)$ with its coordinates rotated by a further $2\pi/m$, and thus it is given parametrically by

$$\gamma(t) = (r\cos[2(\psi t - 2\pi)/m], r\sin[2(\psi t - 2\pi)/m], bt/m). \tag{6}$$

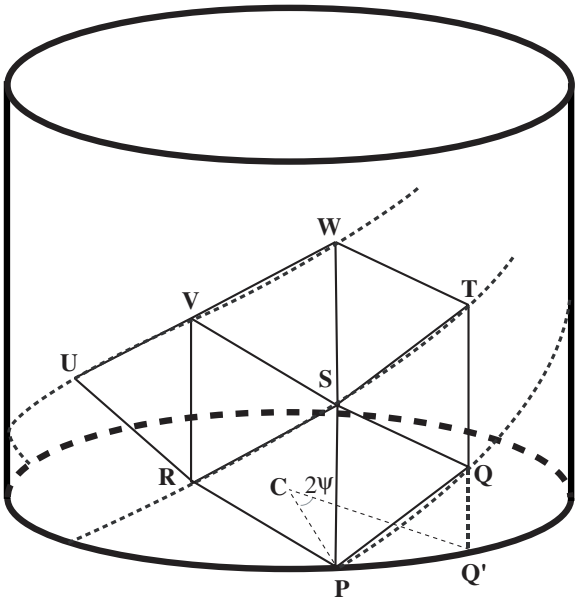

Figure 3. Points lying on three helices and forming an equilateral triangle in three-dimensional space.

From figure 3, the two points **P** and **Q** lie on the first helix $\alpha(t)$, where $\mathbf{P} = \alpha(0) = (r, 0, 0)$ in Cartesian coordinates and the point $\mathbf{Q} = \alpha(m) = (r\cos 2\psi, r\sin 2\psi, b)$. Therefore the distance of the bond length σ joining these two points is given by $\sigma^2 = 4r^2\sin^2\psi + b^2$.

Likewise, the points **R**, **S** and **T** lie on the second helix $\beta(t)$ and the points **U**, **V** and **W** lie on the third helix $\gamma(t)$, where $\mathbf{R} = \beta(n)$, $\mathbf{S} = \beta(n+m)$, $\mathbf{T} = \beta(n+2m)$, $\mathbf{U} = \gamma(2n)$, $\mathbf{V} = \gamma(2n+m)$ and $\mathbf{W} = \gamma(2n+2m)$. The three points of **P**, **R** and **S** comprise one equilateral triangle, and from postulate (i), we require all edges of that triangle to be equal, and therefore $|\mathbf{PR}| = |\mathbf{PS}| = |\mathbf{RS}| = \sigma$ and from the parametric equations (4)–(6) we may derive the following expressions

$$
\begin{aligned}
|\mathbf{PQ}|^2 &= |\mathbf{RS}|^2 = 4r^2\sin^2\psi + b^2,\\
|\mathbf{PR}|^2 &= 4r^2\sin^2\xi + (nb/m)^2,\\
|\mathbf{PS}|^2 &= 4r^2\sin^2(\xi+\psi) + [(n+m)b/m]^2,
\end{aligned}
$$

where $\xi = (n\psi - \pi)/m$ and from postulate (i), we require $|\mathbf{PQ}| = |\mathbf{PR}|$ and $|\mathbf{PQ}| = |\mathbf{PS}|$ and therefore we may derive

$$
\begin{aligned}
b^2/r^2 &= 4m^2(\sin^2\psi - \sin^2\xi)/(n^2 - m^2),\\
b^2/r^2 &= 4m^2[\sin^2\psi - \sin^2(\xi+\psi)]/(n^2 + 2nm).
\end{aligned}
\tag{7}
$$

The fundamental parameter of the polyhedral model is the subtend semi-angle ψ which is derived from (7), and the transcendental equation for ψ is given by

$$
(n^2 - m^2)\sin^2(\xi+\psi) - n(n+2m)\sin^2\xi + m(2n+m)\sin^2\psi = 0, \tag{8}
$$

where $\xi = (n\psi - \pi)/m$. The subtend semi-angle ψ is determined as a root of (8), which may have many roots, but based on geometric considerations, the subtend semi-angle ψ must

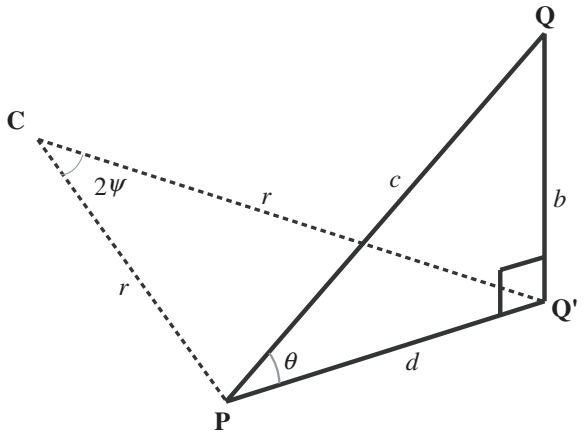

Figure 4. Points forming **PQQ′** in three-dimensional space.

also satisfy the inequalities (9), since $\xi \leqslant 0 \leqslant (\xi + \psi)$. Thus, for a physically meaningful structure the subtend semi-angle ψ satisfies the following inequalities:

$$\pi/(n+m) \leqslant \psi \leqslant \pi/n. \tag{9}$$

Equation (8) is a transcendental equation which cannot be solved explicitly for arbitrary n and m. However, an accurate numerical value for the required root of (8) may be determined after a small number of iterations of Newton's method, using an initial value of $\psi_0 = \pi(2n+m)/[2(n^2+nm+m^2)]$. Equation (8) does have simple exact analytical solutions for particular values of n and m, and specifically we may show that $\psi = \pi/n$ when $m = 0$, and $\psi = \pi/(2n)$ when $m = n$.

The true chiral angle θ is found by considering a triangle comprising the points **P**, **Q** and the point **Q′**, which is determined by projecting **Q** onto the xy-plane as shown in figure 4. Therefore, the distance c^2 is given by

$$c^2 = 4r^2(n^2 \sin^2\psi - m^2 \sin^2\xi)/(n^2 - m^2). \tag{10}$$

With reference to figure 4, the distance d is deduced from the cosine law, and is given by

$$d = 2r \sin\psi. \tag{11}$$

The result of this derivation is that the true chiral angle θ is given by

$$\cos^2\theta = \frac{n(n+2m)\sin^2\psi}{(n+m)^2\sin^2\psi - m^2\sin^2(\xi+\psi)}. \tag{12}$$

We note that from (7) we have two expressions for b^2 and hence the true chiral angle θ can also be expressed in the same form given in (12) where c^2 is given by

$$c^2 = 4r^2[(n+m)^2\sin^2\psi - m^2\sin^2(\xi+\psi)]/(n^2+2nm). \tag{13}$$

The adjacent bond angle ϕ is defined as the angle between two bonds where the three bonded atoms comprise a single triangle in the nanotube lattice. The next neighbour bond angles are for the angles between two bonds which are not adjacent and not opposite, that is they have one bond separating them. The three opposite bond angles are the angles between two bonds where the atoms being bonded are collinear in the flat nanotube lattice. Expressions for the adjacent bond angle ϕ, the next neighbour bond angles ω_1, ω_2 and ω_3 and the three

opposite bond angles μ_1, μ_2 and μ_3, may be derived from the cosine law. Since the bonds are assumed to be all the same length from postulate (i), $\triangle$**PQS** is equilateral therefore the adjacent bond angle $\phi \equiv 60^\circ$. The next neighbour bond angles are determined from distinct triangles, where the angle ω_1 is found from the triangle $\triangle$**PSV**, ω_2 is found from the triangle $\triangle$**RSQ** and ω_3 is found from the triangle $\triangle$**PST**. Similarly, the three opposite bond angles μ_1, μ_2 and μ_3 are found from the triangles $\triangle$**VSQ**, $\triangle$**RST** and $\triangle$**PSW**, respectively. There are three next neighbour bond angles ω_1, ω_2 and ω_3 are found to be

$$\begin{aligned}
\cos\omega_1 &= 1 - \frac{1}{2}\left[\frac{\cos^2\theta\sin^2(2\xi+\psi)}{\sin^2\psi} + \frac{(2n+m)^2\sin^2\theta}{m^2}\right],\\
\cos\omega_2 &= 1 - \frac{1}{2}\left[\frac{\cos^2\theta\sin^2(\xi-\psi)}{\sin^2\psi} + \frac{(n-m)^2\sin^2\theta}{m^2}\right],\\
\cos\omega_3 &= 1 - \frac{1}{2}\left[\frac{\cos^2\theta\sin^2(\xi+2\psi)}{\sin^2\psi} + \frac{(n+2m)^2\sin^2\theta}{m^2}\right].
\end{aligned} \tag{14}$$

The three opposite bond angles μ_1, μ_2 and μ_3 are given by

$$\begin{aligned}
\cos\mu_1 &= 1 - \frac{1}{2}\left[\frac{\cos^2\theta\sin^2(2\xi)}{\sin^2\psi} + \frac{4n^2\sin^2\theta}{m^2}\right],\\
\cos\mu_2 &= 1 - \frac{1}{2}\left[\frac{\cos^2\theta\sin^2(2\psi)}{\sin^2\psi} + \frac{4m^2\sin^2\theta}{m^2}\right],\\
\cos\mu_3 &= 1 - \frac{1}{2}\left[\frac{\cos^2\theta\sin^2[2(\xi+\psi)]}{\sin^2\psi} + \frac{4(n+m)^2\sin^2\theta}{m^2}\right].
\end{aligned} \tag{15}$$

As a natural consequence of the polyhedral model, boron nanotubes may be viewed as having a wall thickness arising from two radii, an outer and an inner radius of the polyhedron. The outer radius r is taken to be the distance of every boron atom from the nanotube axis, in other words it coincides with the nanotube radius. The closest perpendicular distance of all bonds and the nanotube axis is adopted as the perceived inner radius r_{in}. Thus, a hollow cylinder of radii r and r_{in} is precisely the smallest such cylinder which can enclose all the atoms and all the bonds of the nanotube. The nanotube radius r is the distance from the boron atoms to the nanotube axis which may be found from $\cos\theta$ and the length of **PQ**, which is the boron–boron covalent bond length, since $|\mathbf{PQ}| = c = \sigma$. As can be seen from figure 4, $\cos\theta = d/c$ where d is given by (11), and therefore the nanotube radius and inner radius are given by

$$r = (\sigma\cos\theta)/(2\sin\psi), \qquad r_{\text{in}} = r\cos\psi, \tag{16}$$

where σ is the length of the boron–boron bond. The inner radius r_{in} is the minimum distance between the nanotube axis and the midpoint of the closest boron–boron bond. The nanotube thickness δ is taken as the difference between r and r_{in}, and is given by

$$\delta = [\sigma\cos\theta\tan(\psi/2)]/2. \tag{17}$$

The boron nanotubes examined here may be considered to be constructed from a repeating unit cell. The rectangle **OAB′B** shown in figure 2, is the unit cell and contains a number of atoms N given by $N = |\mathbf{C_h}\times\mathbf{T}|/|\mathbf{a_1}\times\mathbf{a_2}|$. Thus the number of atoms in the unit cell for the polyhedral model is found as

$$N = 2(n^2+nm+m^2)/d_R.$$

The unit cell length L is the total number of atoms from a unit cell in a single helix multiplied the helical vertical spacing coefficient b. The total number of atoms in a single helix is found

from the number of atoms in a unit cell N divided by the number of helices m. Thus the unit cell length is given by $L = Nb/m$ which by substitution leads to

$$L = [2\sigma(n^2 + nm + m^2)\sin\theta]/(md_R). \tag{18}$$

3. Asymptotic expansions for the polyhedral model

The equations of the polyhedral model may be expressed in terms of $1/n$ in the limit of $n \to \infty$ by using the method of asymptotic expansions described in appendix A. The subtend semi-angle ψ determined from the transcendental equation (8) is given by

$$\psi = \frac{\pi(2n+m)}{2\Delta} + \frac{3\pi^3 nm^2(n^2-m^2)(2n+m)(n+2m)}{32\Delta^5} + O\left(\frac{1}{n^5}\right), \tag{19}$$

where $\Delta = (n^2 + nm + m^2)$ and the $O(1/n)$ term refers the maximum order of the magnitude of the next most significant term. The dominant behaviour of the subtend semi-angle ψ is given by the leading term of (19), and the second term may be viewed as a correction term that takes into account the curvature of the nanotube. The subtend semi-angle ψ can also be expressed as a series using the Lagrange expansion which is given by

$$\psi = \sum_{k=0}^{\infty} \frac{1}{(2k+1)!}\left[\frac{\mathrm{d}^{2k}}{\mathrm{d}\Psi^{2k}}\left(\frac{\pi\Psi}{n\Psi + m\tan^{-1}(\lambda)}\right)^{2k+1}\right]_{\Psi=0}, \tag{20}$$

where λ is given by the expression

$$\lambda = \frac{n(n+2m)\tan\Psi}{n^2 - m^2 + \nu^{1/2}},$$

$$\nu = (n^2-m^2)[n^2 - m^2 + n(n+2m)\tan^2\Psi] + nm(n+2m)(2n+m).$$

It is worth commenting that up to this order, (19) and (20) are totally in accordance with the special cases of armchair nanotubes $n = m$, where $\psi = \pi/(2n)$, as well as the case of zigzag nanotubes $m = 0$, where $\psi = \pi/n$.

By substituting (19) into the expression for the chiral angle θ given in (12) and then by further expansion in terms of $1/n$, an expansion for $\cos^2\theta$ may be developed which is given by

$$\cos^2\theta = \frac{(2n+m)^2}{4\Delta} + \frac{\pi^2 m^2(2n+m)^2(n+2m)^2(n-m)^2}{64\Delta^5} + O\left(\frac{1}{n^4}\right), \tag{21}$$

where the first term is exactly the conventional expression of the chiral angle θ_0 as given in (1), and the second term is a first-order correction to the conventional chiral angle θ_0. We may also express (21) in terms of the conventional chiral angle θ_0 and the conventional radius r_0, as given in (3), and we may show that

$$\cos^2\theta = \cos^2\theta_0 + \frac{\sigma^2\sin^2\theta_0}{96r_0^2}[1 + \cos(6\theta_0)] + O\left(\frac{1}{n^4}\right). \tag{22}$$

Expansions for the three next neighbour bond angles ω_1, ω_2 and ω_3, are developed by substituting (19) and (21) into three exact formulae (14) and then by further expansion we may derive

$$\cos\omega_1 = -\frac{1}{2} + \frac{\pi^2(n+2m)^2(n-m)^2}{8\Delta^3} + O\left(\frac{1}{n^4}\right),$$

$$\cos\omega_2 = -\frac{1}{2} + \frac{\pi^2(2n+m)^2(n+2m)^2}{8\Delta^3} + O\left(\frac{1}{n^4}\right),$$

$$\cos\omega_3 = -\frac{1}{2} + \frac{\pi^2(2n+m)^2(n-m)^2}{8\Delta^3} + O\left(\frac{1}{n^4}\right).$$

Similarly, the expansions of the three opposite bond angles μ_1, μ_2 and μ_3, are found by substitution of (19) and (21) into (15) from which the expansions for $\cos\mu_1$, $\cos\mu_2$ and $\cos\mu_3$ are given by

$$\cos\mu_1 = -1 + \frac{\pi^2(n+2m)^4}{8\Delta^3} + O\left(\frac{1}{n^4}\right),$$
$$\cos\mu_2 = -1 + \frac{\pi^2(2n+m)^4}{8\Delta^3} + O\left(\frac{1}{n^4}\right),$$
$$\cos\mu_3 = -1 + \frac{\pi^2(n-m)^4}{8\Delta^3} + O\left(\frac{1}{n^4}\right).$$

The asymptotic expansions of the nanotube radius r, the thickness δ and the unit cell length L may be developed using the same technique, and the nanotube radius r is given by

$$r = \frac{\sigma\sqrt{\Delta}}{2\pi} + \frac{\pi\sigma[16\Delta^3 - 27n^2m^2(n+m)^2]}{192\Delta^{7/2}} + O\left(\frac{1}{n^3}\right), \tag{23}$$

where the leading order term is exactly the conventional expression given in (3). Similarly, we may show that the second term is a first-order correction to the conventional radius r_0 and takes into account the curvature of the structure. Equation (23) may also be written in terms of the conventional radius r_0 and chiral angle θ_0 given by (1) and (3), which leads to

$$r = r_0 + \frac{\sigma^2}{192r_0}[7 + \cos(6\theta_0)] + O\left(\frac{1}{n^3}\right). \tag{24}$$

Following the same method, the asymptotic expansions of the thickness δ is given by

$$\delta = \frac{\pi\sigma(2n+m)^2}{16\Delta^{3/2}} + \frac{\pi^3\sigma(2n+m)^2(8\Delta^3 + 15m^2\Delta^2 - 9m^4\Delta - 81nm^4(n+m))}{1536\Delta^{11/2}} + O(1/n^5). \tag{25}$$

Both terms in (25) are new, since there is at present no widely accepted theory on the nanotube thickness. The order of the leading term is $1/n$ and so the thickness δ approaches zero as the size of the nanotube increases. This is expected since the thickness used here is a measure of the curvature of the facetted surface model. We also note that the thickness can be approximated by the relation

$$\delta = (\sigma^2\cos^2\theta_0)/(8r_0) + O(1/n^3). \tag{26}$$

Finally, the unit cell length L is given by the expansion

$$L = \frac{\sigma\sqrt{3\Delta}}{d_R} - \frac{\sqrt{3}\sigma\pi^2(2n+m)^2(n+2m)^2(n-m)^2}{96\Delta^{7/2}d_R} + O\left(\frac{1}{n^3}\right), \tag{27}$$

where the first term also is precisely the conventional expression given in (2) and the second term is a first-order correction to the conventional unit cell length L_0 incorporating the curvature of the structure, and which may be expressed in terms of the conventional parameters as

$$L = L_0 - \frac{\sqrt{3}\sigma^2\pi}{96r_0d_R}[1 + \cos(6\theta_0)] + O\left(\frac{1}{n^3}\right). \tag{28}$$

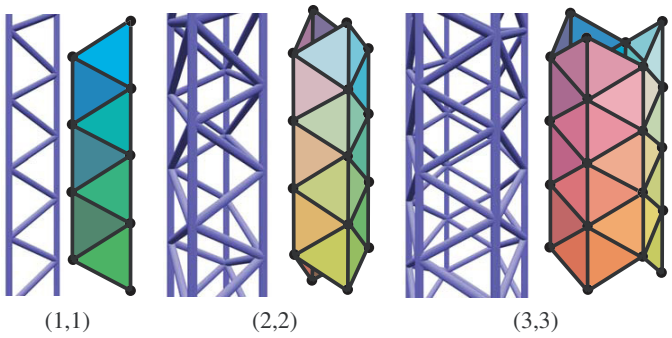

Figure 5. (1, 1), (2, 2), (3, 3) armchair boron nanotubes.

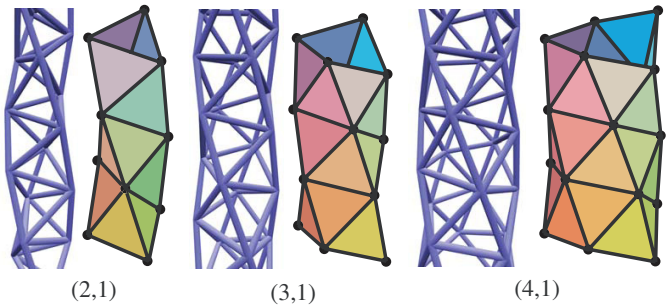

Figure 6. (2, 1), (3, 1), (4, 1) chiral boron nanotubes.

4. Geometric structure of ultra-small boron nanotubes

In this section we consider the structure of boron nanotubes in the limit of decreasing radius. In some cases counterintuitive geometric structures arise and in other cases, the nanotube cannot be constructed at all. The ultra-small boron nanotubes considered here are illustrated by two representations shown in figures 5–7, where the figure on the left is a perspective drawing of bonds, and that on the right shows the tube where the triangular lattice elements are shown as shaded patches. Figure 5 shows (1, 1), (2, 2) and (3, 3) nanotubes for the polyhedral model which are all of the armchair type. The (1, 1) is ladder like but since in our model all the boron nanotubes are assumed to comprise six-coordinated atoms, the present model does not apply for (1, 1) tubes. The (2, 2) and (3, 3) tubes show $2n$-sided polygonal tubes.

We illustrate two chiral nanotubes of types (2, 1), (3, 1) and (4, 1) in figure 6. The (2, 1) tube clearly shows that the surface of the nanotube is not smooth when the bonds are assumed to be straight lines. The (3, 1) and (4, 1) tubes are also facetted but they appear smoother due to the less extreme curvature of the tube surface.

Zigzag boron nanotubes are shown in figure 7. As expected (4, 0) has a square tube shape and (3, 0) has a triangular structure. The (2, 0) nanotube shows a very facetted structure which arises from the extreme curvature present in that structure. The structure of the (2, 0) tube appears somewhat like a toy snake and comprises nodes formed from the triangular lattice elements for which the joins arise from the arrangement of the double bonds components but since it has double bonds, the present model does not apply for (2, 0) tubes. Ultra-small boron

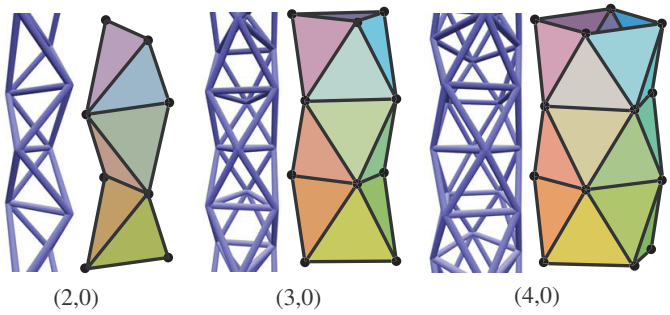

Figure 7. (2, 0), (3, 0), (4, 0) zigzag boron nanotubes.

nanotubes tend not to be produced in experiments due to their highly facetted structure and the formation energy may be too high. Also small nanotubes may exhibit distinct bond lengths which is not accounted for in this model. Very large nanotubes do not occur in experiments and therefore the radii of nanotubes tend to lie in a definite range.

5. Results

Many different values for the boron–boron bond length σ have been reported in the literature which range from 1.6 and 1.85 Å [10, 13, 22]. Many studies adopt $\sigma = 1.67$ Å for the flat triangular lattice [16, 21, 24, 26] and for the stable B_{80} fullerene [12, 27] and in the present work we adopt this particular value. In table 1 we present results for the subtend angle 2ψ, true chiral angle θ, next neighbour bond angles ω_1, ω_2 and ω_3, opposite bond angles μ_1, μ_2 and μ_3, nanotube radius r, length L and thickness δ for a variety of nanotubes for $2 \leqslant n \leqslant 6$.

We now compare our results with the studies of Cabria *et al* [21, 25] and of Lau *et al* [11]. Table 2 shows a comparison of radius with Cabria *et al* [21, 25] and indicates that the results of the polyhedral model are in excellent agreement. Similarly, table 3 shows a comparison of radius with Lau *et al* [11] and shows that the results of the polyhedral model are also in agreement. We emphasize that the data shown in the final column of table 4 arise from Yang *et al* [27] and Yang [28] upon averaging three distinct radii and the comparison is with a different lattice structure involving both triangles and hexagons.

Figure 8 shows a plot of the subtend angle 2ψ versus n, and shows that the subtend angle increases rapidly as the value of n decreases. This occurs due to the increasing curvature of the tube surface as n decreases, since the nanotubes with the smallest values of n have the largest curvature. We see from figure 9 that the values of the chiral angle for zigzag and armchair are constant with the values 0° and 30° respectively. In these two extreme cases, the chiral angle is independent of n, for both the conventional model and the polyhedral model. The same behaviour exists for carbon nanotubes in the polyhedral model [32]. Figure 9 also shows that the value of the chiral angle θ for $(n, n/2)$ tubes is almost but not exactly constant. In the conventional model, the value of the chiral angle θ_0 is independent of n when the value of m is a constant ratio of n. However, the chiral angle in the polyhedral model has a correction term which takes into account the curvature of the tube surface but the effect of the correction term is not apparent from figure 9. The values of the chiral angle θ for $(n, 1)$ and $(n, n-1)$ tubes asymptote to 0° and 30°, respectively, in the limit as n becomes large. When the value of m is less than a half of $n(m < n/2)$, the value of the chiral angle asymptotes to 0°. When

Table 1. Results of polyhedral model using $\sigma = 1.67$ Å.

(n, m)	2ψ (°)	θ (°)	ω_1 (°)	ω_2 (°)	ω_3 (°)	μ_1 (°)	μ_2 (°)	μ_3 (°)	r (Å)	L (Å)	δ (Å)
(2, 1)	131.81	18.44	112.89	60.00	109.46	109.47	60.00	169.05	0.868	7.394	0.513
(2, 2)	90.00	30.00	120.00	75.52	120.00	104.48	104.48	180.00	1.023	1.670	0.300
(3, 0)	120.00	0.00	109.47	90.00	90.00	146.44	60.00	146.44	0.964	2.727	0.482
(3, 1)	97.74	13.57	115.35	85.86	111.42	134.00	85.86	169.44	1.078	10.190	0.369
(3, 2)	76.31	23.33	119.25	90.35	119.02	128.39	110.88	178.50	1.241	12.568	0.265
(3, 3)	60.00	30.00	120.00	97.18	120.00	128.68	128.68	180.00	1.446	1.670	0.194
(4, 0)	90.00	0.00	114.47	101.95	101.95	156.09	90.00	156.09	1.181	2.809	0.346
(4, 1)	77.41	10.72	116.81	98.67	113.22	146.98	104.18	170.12	1.312	4.348	0.288
(4, 2)	64.61	19.01	118.90	99.86	118.30	142.02	119.30	177.07	1.477	7.615	0.229
(4, 3)	53.66	25.26	119.82	102.98	119.78	140.56	131.82	179.53	1.673	17.581	0.180
(4, 4)	45.00	30.00	120.00	106.28	120.00	141.29	141.29	180.00	1.890	1.670	0.144
(5, 0)	72.00	0.00	116.57	108.00	108.00	161.30	108.00	161.30	1.421	2.841	0.271
(5, 1)	63.98	8.84	117.71	105.69	114.61	154.67	116.87	170.84	1.557	15.920	0.237
(5, 2)	55.56	16.02	118.91	105.80	118.08	150.55	126.77	176.26	1.722	5.990	0.198
(5, 3)	47.88	21.75	119.63	107.23	119.49	148.64	135.71	178.82	1.911	20.215	0.164
(5, 4)	41.37	26.32	119.93	109.10	119.92	148.32	143.09	179.79	2.119	22.585	0.137
(5, 5)	36.00	30.00	120.00	110.90	120.00	148.96	148.96	180.00	2.340	1.670	0.115
(6, 0)	60.00	0.00	117.65	111.47	111.47	164.60	120.00	164.60	1.670	2.858	0.224
(6, 1)	54.47	7.52	118.29	109.86	115.66	159.64	126.04	171.53	1.809	18.805	0.201
(6, 2)	48.56	13.83	119.02	109.62	118.10	156.27	132.94	175.85	1.972	10.380	0.174
(6, 3)	42.95	19.07	119.55	110.27	119.30	154.35	139.51	178.24	2.156	7.637	0.150
(6, 4)	37.95	23.40	119.85	111.32	119.80	153.57	145.27	179.41	2.357	12.600	0.128
(6, 5)	33.65	26.99	119.97	112.47	119.97	153.58	150.11	179.89	2.570	27.590	0.110
(6, 6)	30.00	30.00	120.00	113.55	120.00	154.09	154.09	180.00	2.794	1.670	0.095

Table 2. Comparison of radii from conventional model, polyhedral model and local density approximation method of Cabria *et al* [21, 25].

(n, m)	σ (Å)	Radius r_0 (Å)	Radius r (Å)	Cabria *et al* [21, 25] (Å)
(12, 0)	1.72	3.285	3.323	3.35
(15, 0)	1.71	4.082	4.112	4.12

Table 3. Comparison of radii from conventional model, polyhedral model and density functional theory study of Lau *et al* [11] using $\sigma = 1.68$ Å.

(n, m)	Radius r_0 (Å)	Radius r (Å)	Lau *et al* [11] (Å)
(6, 0)	3.209	3.360	3.3

$m > n/2$, the chiral angle asymptotes to 30° in the limit of increasing n. When $m = n/2$, the value of the chiral angle starts from 18.44° and asymptotes to 19.11° in the limit of increasing n, where 19.11° is the chiral angle arising in the conventional model.

The adjacent bond angle ϕ is a constant 60° for any value of n and m in both models. The plot of the next neighbour bond angles ω_1, ω_2 and ω_3 versus n are shown in figures 10–12. The next neighbour bond angles asymptote to 120° in the limit as n becomes large, except for ω_1 and ω_3 for the armchair tubes because their values are constant at 120°. Similarly, figures 13–15 show that all opposite bond angles μ_1, μ_2 and μ_3 asymptote to 180° in the limit as n

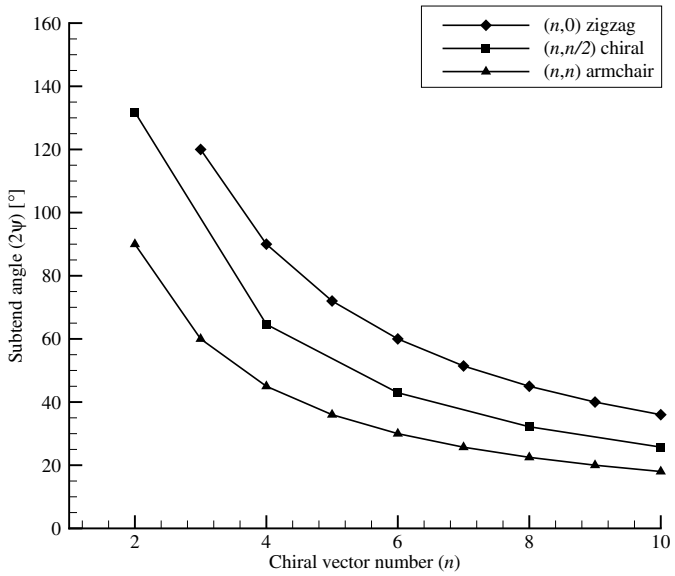

Figure 8. Subtend angle 2ψ for boron nanotubes of type zigzag: (3, 0)–(10, 0), chiral: (2, 1)–(10, 5) and armchair: (2, 2)–(10, 10).

Table 4. Comparison of radii from conventional model, polyhedral model and first-principles method of Yang *et al* [27, 28] using $\sigma = 1.67$ Å.

(n, m)	Radius r_0 (Å)	Radius r (Å)	Yang *et al* [28] (Å)
(12, 0)	3.189	3.226	3.242
(15, 0)	3.987	4.016	4.036
(18, 0)	4.784	4.809	4.836
(21, 0)	5.582	5.602	5.634
(24, 0)	6.379	6.397	6.431
(27, 0)	7.176	7.193	7.229
(9, 9)	4.143	4.164	4.180
(12, 12)	5.524	5.540	5.568
(15, 15)	6.905	6.918	6.944
(18, 18)	8.286	8.297	8.329
(21, 21)	9.668	9.677	9.736

becomes large, except for μ_3 for the armchair tube, since they are constant at 180° in the limit of increasing n. These phenomena for the next neighbour bond angles and the opposite bond angles arise since the surface of the nanotubes approach a flat plane in the limit of increasing n.

The percentage difference between the nanotube radii of the conventional model and the polyhedral model $(r - r_0)/r_0 \times 100\%$ is shown in figure 16. As n decreases, the percentage difference in radii increases, due to the increasing curvature of the nanotube. As n becomes large, the curvature becomes insignificant and the two models converge. The percentage difference for the radii between the polyhedral model and the conventional model is less then 5%, when $n + m \geqslant 7$, except for the (6, 0) and (3, 3) tubes. This percentage difference is less

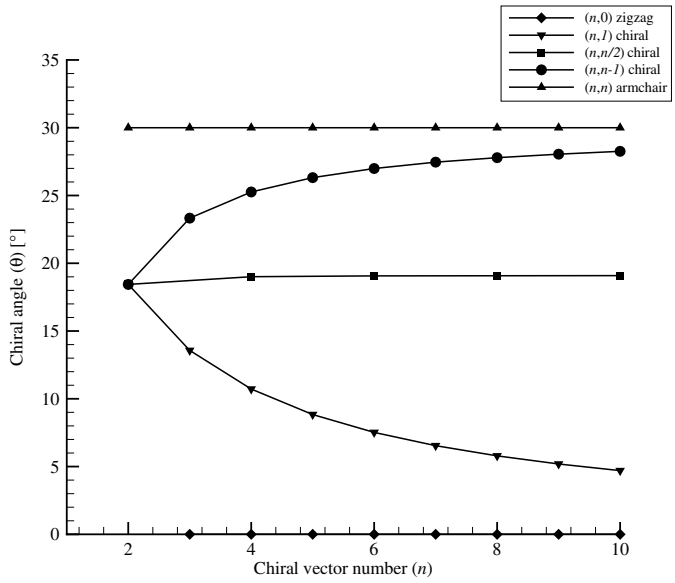

Figure 9. Chiral angle θ for boron nanotubes of type zigzag: (3, 0)–(10, 0), chiral: (2, 1)–(10, 1), (2, 1)–(10, 5) and (2, 1)–(10, 9) and armchair: (2, 2)–(10, 10).

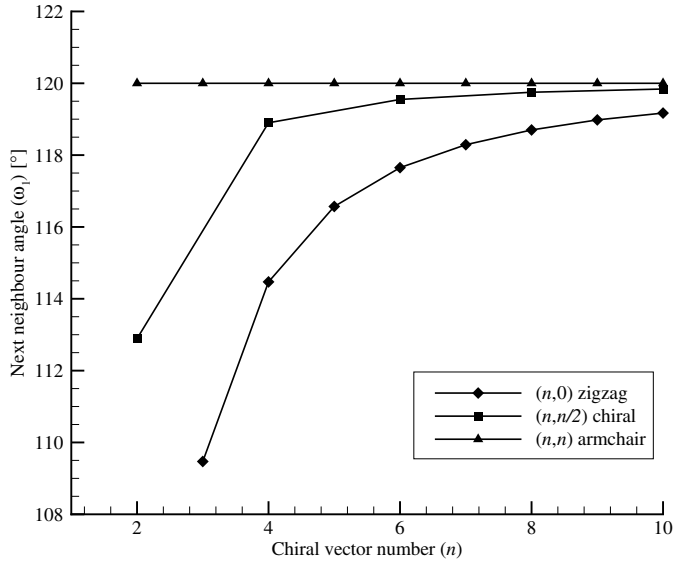

Figure 10. Next neighbour bond angle ω_1 for boron nanotubes of type zigzag: (3, 0)–(10, 0), chiral: (2, 1)–(10, 5) and armchair: (2, 2)–(10, 10).

than 2%, when $n + m \geqslant 10$. Figure 17 shows the percentage difference between the unit cell length of the conventional model and the polyhedral model $(L - L_0)/L_0 \times 100\%$. There is no difference between the two models for the unit cell length for armchair tubes. However, zigzag nanotubes display the maximum difference for the unit cell length, as n becomes small. Chiral

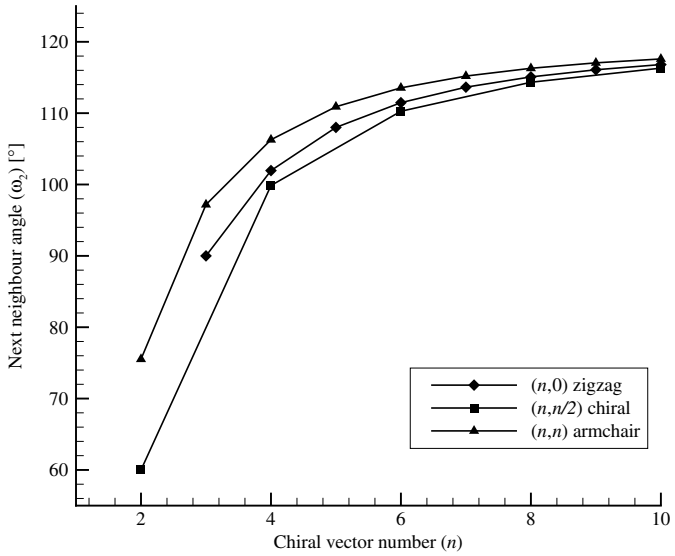

Figure 11. Next neighbour bond angle ω_2 for boron nanotubes of type zigzag: (3, 0)–(10, 0), chiral: (2, 1)–(10, 5) and armchair: (2, 2)–(10, 10).

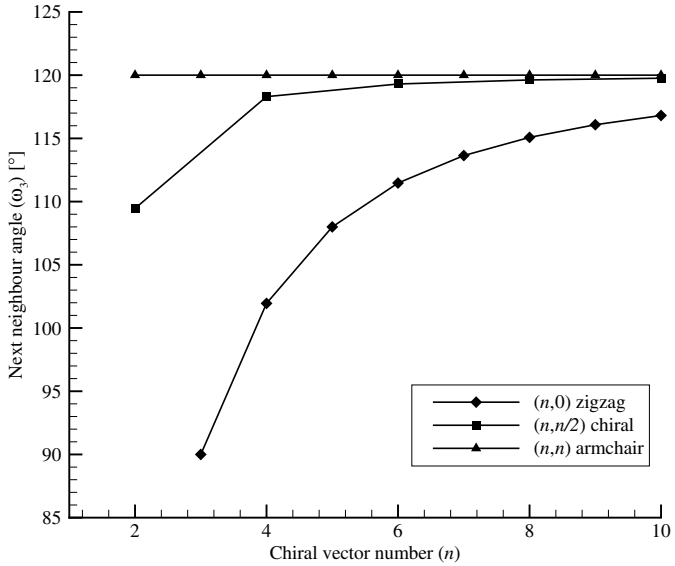

Figure 12. Next neighbour bond angle ω_3 for boron nanotubes of type zigzag: (3, 0)–(10, 0), chiral: (2, 1)–(10, 5) and armchair: (2, 2)–(10, 10).

tubes exhibit behaviour that is between the armchair and the zigzag tubes. The percentage difference is negative, which signifies that the unit cell length L is shorter than the conventional unit cell length L_0.

Figures 18 and 19 show plots of nanotube thickness δ versus n for boron nanotubes and carbon nanotubes for the polyhedral model respectively. Both plots show similar trends

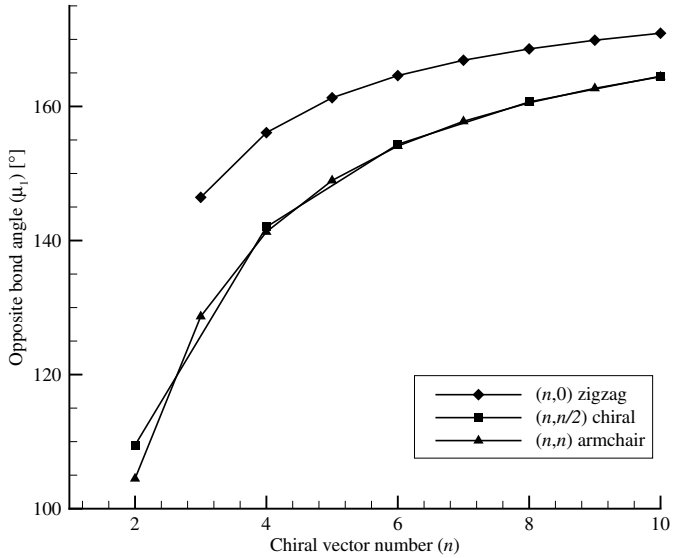

Figure 13. Opposite bond angle μ_1 for boron nanotubes of type zigzag: (3, 0)–(10, 0), chiral: (2, 1)–(10, 5) and armchair: (2, 2)–(10, 10).

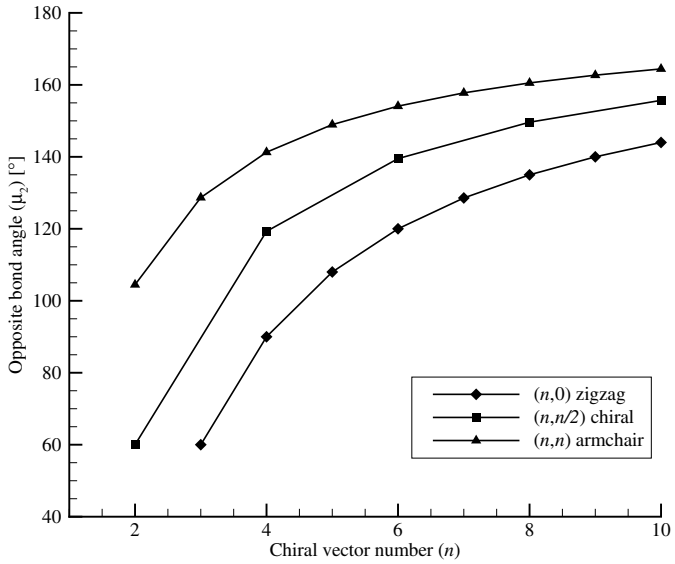

Figure 14. Opposite bond angle μ_2 for boron nanotubes of type zigzag: (3, 0)–(10, 0), chiral: (2, 1)–(10, 5) and armchair: (2, 2)–(10, 10).

because as n becomes small, the nanotube thickness becomes larger and similarly, when n becomes large, the thickness approaches zero. Therefore the thickness of the polyhedral model is curvature related and becomes significant for ultra-small nanotubes.

By examining the asymptotic expansions of the expressions for the polyhedral model for the chiral angle (22), the radius (24) and the unit cell length (28) we observe that the leading

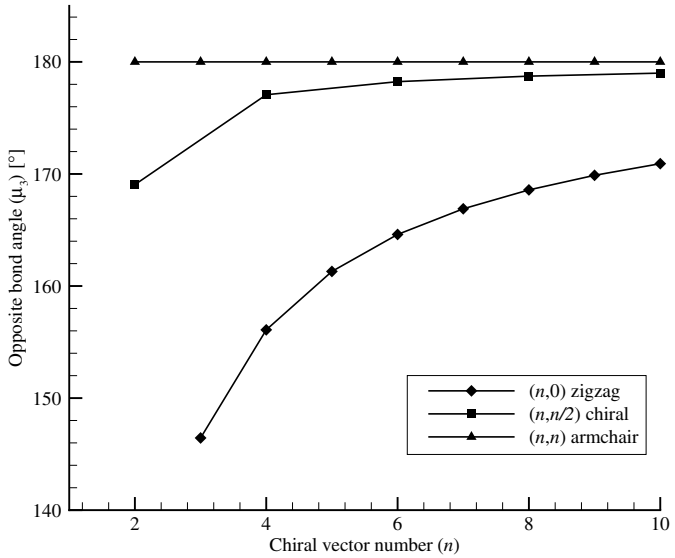

Figure 15. Opposite bond angle μ_3 for boron nanotubes of type zigzag: (3, 0)–(10, 0), chiral: (2, 1)–(10, 5) and armchair: (2, 2)–(10, 10).

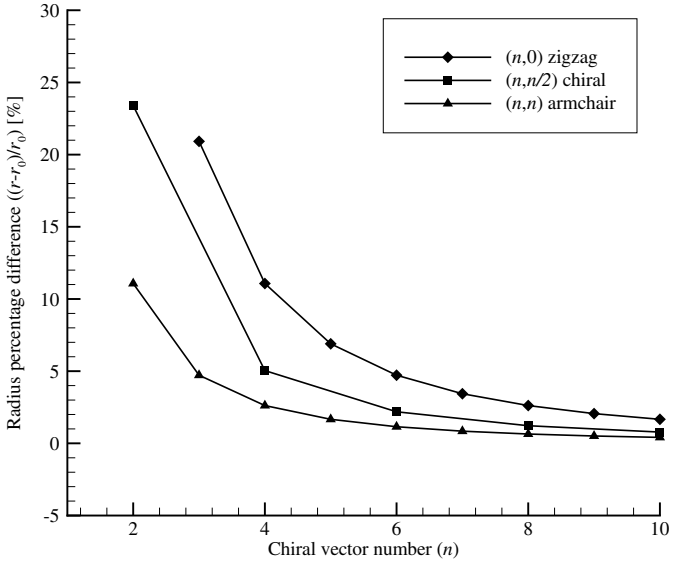

Figure 16. Percentage difference between the polyhedral model and the conventional radius $((r - r_0)/r_0)$ [%] for boron nanotubes of type zigzag: (1, 0)–(10, 0), chiral: (2, 1)–(10, 5) and armchair: (1, 1)–(10, 10).

order terms of the analytical expressions are the conventional formulae while the second-order terms may be viewed as corrections to the conventional model, which are of order $1/n$ or smaller. This demonstrates that the polyhedral model converges to the conventional model in the limit of increasing n.

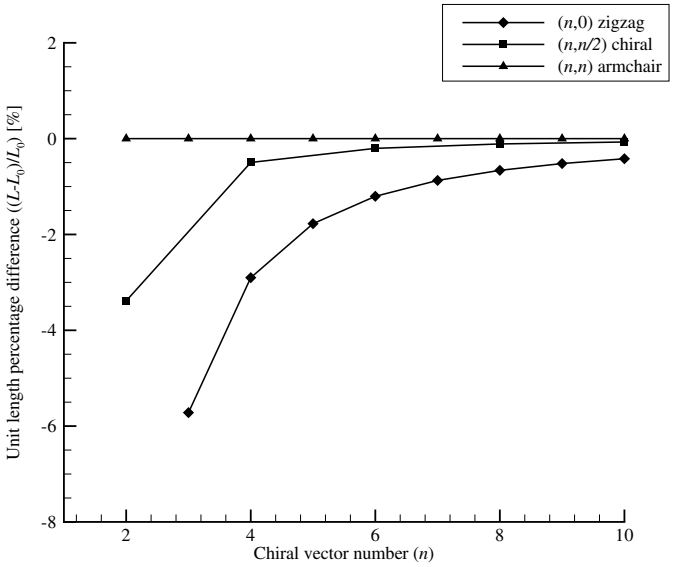

Figure 17. Percentage difference between the polyhedral model and the conventional unit cell length $((L - L_0)/L_0)$ [%] for boron nanotubes of type zigzag: (1, 0)–(10, 0), chiral: (2, 1)–(10, 5) and armchair: (1, 1)–(10, 10).

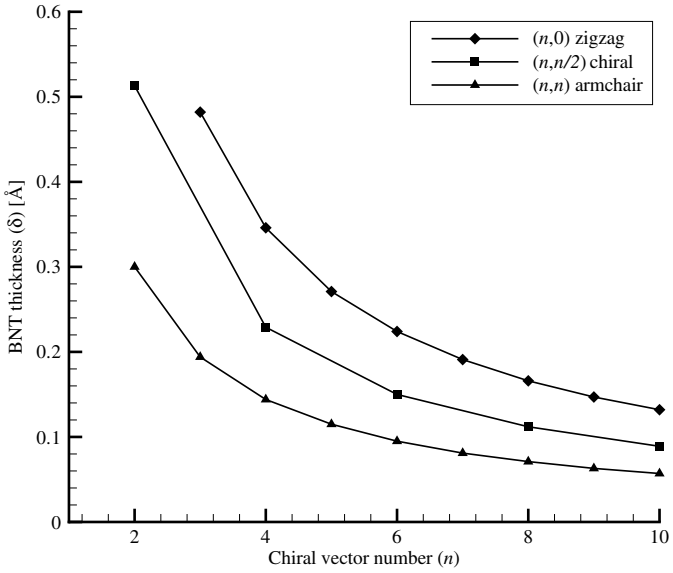

Figure 18. Thickness δ for boron nanotubes of type zigzag: (3, 0)–(10, 0), chiral: (2, 1)–(10, 5) and armchair: (2, 2)–(10, 10).

6. Conclusions

Boron has a very stable lattice structure which is formed from sp^2 hybridized bonds. Here we consider the lattice for boron nanotubes to comprise only equilateral triangles, and we have derived the key geometric parameters that arise in a new polyhedral model of boron

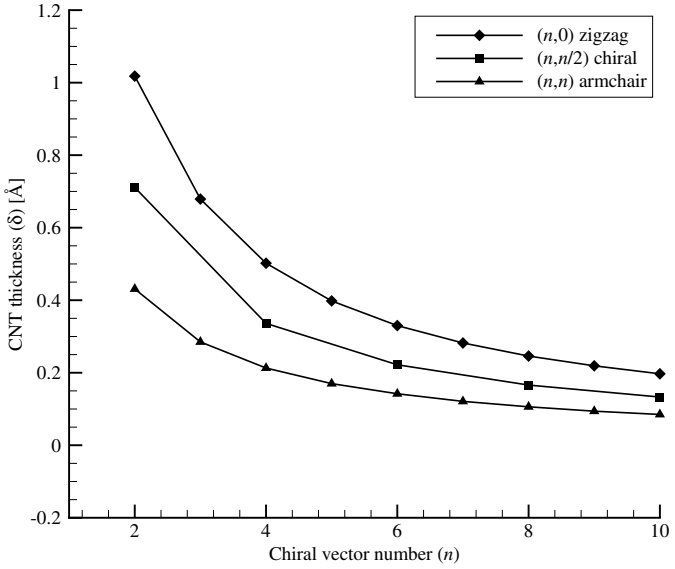

Figure 19. Thickness δ for carbon nanotubes of type zigzag: (2, 0)–(10, 0), chiral: (2, 1)–(10, 5) and armchair: (2, 2)–(10, 10).

Table 5. Main equations for polyhedral model.

Parameter name	Equation
Subtend semi-angle ψ	$(n^2 - m^2)\sin^2(\xi + \psi) - n(n + 2m)\sin^2\xi + m(2n + m)\sin^2\psi = 0$
Chiral angle θ	$\cos^2\theta = \frac{n(n+2m)\sin^2\psi}{(n+m)^2\sin^2\psi - m^2\sin^2(\xi+\psi)}$
Next neighbour bond angle ω_1	$\cos\omega_1 = 1 - \frac{1}{2}\left[\frac{\cos^2\theta\sin^2(2\xi+\psi)}{\sin^2\psi} + \frac{(2n+m)^2\sin^2\theta}{m^2}\right]$
Next neighbour bond angle ω_2	$\cos\omega_2 = 1 - \frac{1}{2}\left[\frac{\cos^2\theta\sin^2(\xi-\psi)}{\sin^2\psi} + \frac{(n-m)^2\sin^2\theta}{m^2}\right]$
Next neighbour bond angle ω_3	$\cos\omega_3 = 1 - \frac{1}{2}\left[\frac{\cos^2\theta\sin^2(\xi+2\psi)}{\sin^2\psi} + \frac{(n+2m)^2\sin^2\theta}{m^2}\right]$
Opposite bond angle μ_1	$\cos\mu_1 = 1 - \frac{1}{2}\left[\frac{\cos^2\theta\sin^2(2\xi)}{\sin^2\psi} + \frac{4n^2\sin^2\theta}{m^2}\right]$
Opposite bond angle μ_2	$\cos\mu_2 = 1 - \frac{1}{2}\left[\frac{\cos^2\theta\sin^2(2\psi)}{\sin^2\psi} + \frac{4m^2\sin^2\theta}{m^2}\right]$
Opposite bond angle μ_3	$\cos\mu_3 = 1 - \frac{1}{2}\left[\frac{\cos^2\theta\sin^2[2(\xi+\psi)]}{\sin^2\psi} + \frac{4(n+m)^2\sin^2\theta}{m^2}\right]$
Nanotube radius r	$r = (\sigma\cos\theta)/(2\sin\psi)$
Inner radius r_{in}	$r_{\text{in}} = r\cos\psi$
Thickness δ	$\delta = [\sigma\cos\theta\tan(\psi/2)]/2$
Number of atoms in unit cell N	$N = 2(n^2 + nm + m^2)/d_R$
Unit cell length L	$L = [2\sigma(n^2 + nm + m^2)\sin\theta]/(md_R)$

nanotubes, which is based on the two fundamental postulates that all bond lengths are equal and that all atoms lie equidistant from a common axis. Analytical expressions for the major geometric parameters of the tube surface, such as the subtend angle 2ψ, the nanotube radius r, the thickness δ and the unit cell length L are given (see table 5). The fundamental variable of this model is the subtend semi-angle ψ from which all the other parameters are derived

and we find that it is given as a root of the transcendental equation (8) and therefore cannot be written as an explicit analytical function of n and m. We again emphasize that although we have adopted all bond lengths to be equal, a similar but more sophisticated polyhedral model might incorporate unequal bond lengths. Our approach here is first to validate the idealized model and then subsequent modifications can be viewed as deviations from the ideal model behaviour.

For ultra-small boron nanotubes, the tube surface has a very large curvature and the nanotubes tend to exhibit a distinct polyhedral structure, noting that the (2, 1), (3, 1), (4, 1), (2, 0) and (3, 0) tubes are particularly polyhedral. We also find that the (1, 1) and (2, 0) tubes do not exist with sp^2 bonded materials. In practice, ultra-small and very large radii nanotubes tend not to arise in experiments and therefore the radii of nanotubes lie in a definite range. Comparisons of the radii of the nanotubes with Cabria *et al* [21, 25] and Lau *et al* [11] show that the radii predicted by the new polyhedral model are in good overall agreement with these studies. We comment that a possible novel stable lattice pattern proposed in [27] comprises both triangular and hexagonal components. However, a detailed examination of the actual numerical data [28] shows that it possesses three distinct radii. On comparison with Yang *et al* [28] and averaging over the three distinct radii show that the radii predicted by the new polyhedral model are in reasonable agreement with these first-principles calculations. We comment that in reality small radii nanotubes may have highly stretched bonds which are different in length in each direction, and that their formation energy may be too high for them to be formed experimentally. We have not incorporated such factors in the present model.

The other major prediction of this model is that for boron nanotubes we may determine a perceived inner radius r_{in} so that from the nanotube radius r, we may determine a nanotube thickness $\delta = r - r_{\text{in}}$, which becomes vanishingly small as the radius increases, but it is significant for very small nanotubes. We also show that the polyhedral model converges to the conventional model for large n, since the leading term of the analytical expressions gives the conventional formulae as the highest order term, and the second term can be viewed as a correction term which is order $1/n$ or smaller. When $n + m \geqslant 7$, except for the (3, 3) and (6, 0) tubes, the percentage difference between the polyhedral model and the conventional model for the radii r is less than 5%. For zigzag and chiral nanotubes, the unit cell length for polyhedral model L is shorter than the conventional unit cell length L_0. The unit cell lengths for armchair nanotubes in both models have the same value and the unit cell length difference is maximized for zigzag tubes.

Acknowledgments

The support of the Australian Research Council, both through the Discovery Project Scheme and for providing an Australian Professorial Fellowship for JMH. is gratefully acknowledged. The authors are also grateful to Dr Xiaobao Yang [28] for providing the actual numerical data used in [27].

Appendix A. Asymptotic expansions of exact formulae

Using a series expansion in powers of $1/n$ the root of the subtend semi-angle ψ in (8) is determined and we then use this as the basis for determining the series expansions for all of the other parameters derived in the pervious section. Firstly, (8) is written in the form

$$(1 - h^2)\sin^2(\psi + \xi) - (1 + 2h)\sin^2\xi + h(2 + h)\sin^2\psi = 0, \tag{A.1}$$

where $\xi = [\psi - \pi/n]/h$ and $h = m/n$. The numbers m and n are assumed to be of the same magnitude, so that h is assumed to be of order one and ψ becomes small as n increases, and therefore (A.1) is expanded in terms of ψ and $1/n$ where we define the series as

$$\psi = \frac{\psi_0(h)}{n} + \frac{\psi_1(h)}{n^3} + \frac{\psi_2(h)}{n^5} + \cdots,$$
$$\cos^2\theta = a_0(h) + \frac{a_1(h)}{n^2} + \frac{a_2(h)}{n^4} + \cdots.$$

For the subtend semi-angle ψ we may derive by the method of asymptotic expansions the following expressions

$$\psi_0(h) = \frac{\pi(2+h)}{2(1+h+h^2)}, \tag{A.2}$$

$$\psi_1(h) = \frac{\pi^3 h^2(1+2h)(2+h)(1-h^2)}{32(1+h+h^2)^5}, \tag{A.3}$$

which gives ψ is in its asymptotic form (19), by substituting for h in (A.2) and (A.3).

Secondly, the equation for $\cos^2\theta$, (12) is extended by substituting the asymptotic expansion of ψ. Finally, the expansion coefficients of the chiral angle are found in terms of h to be given by

$$a_0(h) = \frac{(2+h)^2}{4(1+h+h^2)}, \qquad a_1(h) = \frac{\pi^2 h^2(2+h)^2(1+2h)^2(h-1)^2}{64(1+h+h^2)^5}.$$

Now the next neighbour bond angles ω_1, ω_2 and ω_3 are found from substituting the asymptotic expansions for ψ and $\cos\theta$ in (14) which are given by

$$\cos\omega_1 = -\frac{1}{2} + \frac{\pi^2(1+2h)^2(h-1)^2}{8(1+h+h^2)^3}\frac{1}{n^2} + O\left(\frac{1}{n^4}\right),$$
$$\cos\omega_2 = -\frac{1}{2} + \frac{\pi^2(1+2h)^2(2+h)^2}{8(1+h+h^2)^3}\frac{1}{n^2} + O\left(\frac{1}{n^4}\right),$$
$$\cos\omega_3 = -\frac{1}{2} + \frac{\pi^2(2+h)^2(h-1)^2}{8(1+h+h^2)^3}\frac{1}{n^2} + O\left(\frac{1}{n^4}\right).$$

The series expansion of the opposite bond angles μ_1, μ_2 and μ_3 are found by substituting the series expansion for $\cos^2\theta$ and expanding the asymptotic equation for ψ. As a result, opposite bond angles of the series expansion are given by

$$\cos\mu_1 = -1 + \frac{\pi^2(1+2h)^4}{8(1+h+h^2)^3}\frac{1}{n^2} + O\left(\frac{1}{n^4}\right),$$
$$\cos\mu_2 = -1 + \frac{\pi^2(2+h)^4}{8(1+h+h^2)^3}\frac{1}{n^2} + O\left(\frac{1}{n^4}\right),$$
$$\cos\mu_3 = -1 + \frac{\pi^2(h-1)^4}{8(1+h+h^2)^3}\frac{1}{n^2} + O\left(\frac{1}{n^4}\right).$$

By substitution of the series expansion for $\cos\theta$ in the formula for the nanotube radius r, $(16)_1$ is expanded in a series involving powers of ψ giving

$$r = \sigma C/2\psi + \sigma C\psi/12 + O(\psi^3), \tag{A.4}$$

where $C = \cos\theta$. From (17) and the series for $\tan(\psi/2)$, the thickness δ is obtained in the following form

$$\delta = \sigma C\psi/4 + \sigma C\psi^3/48 + O(\psi^5). \tag{A.5}$$

Finally, the unit cell length L given by (18) can be expressed by the following expansion

$$L = \frac{\sigma\sqrt{3(1+h+h^2)}}{d_R}n - \frac{\sigma\pi^2\sqrt{3}(2+h)^2(h-1)^2(1+2h)^2}{96(1+h+h^2)^{7/2}d_R}\frac{1}{n} + O(1/n^3). \tag{A.6}$$

From (A.4)–(A.6) and the series expansions (19) and (21) for ψ and $C = \cos\theta$, we may produce expansions for the nanotube radius r, the thickness δ and the unit cell length L, which are given by (23), (25) and (27), respectively.

References

[1] Iijima S 1991 Helical microtubules of graphitic carbon *Nature* **354** 56–8

[2] Li B X and Cao P L 2004 Silicon nanorings and nanotubes: a full-potential linear-muffin-tin-orbital molecular-dynamics method study *J. Mol. Struct. (TheoChem)* **679** 127–30

[3] Wang X and Jiang Q 2008 Developing nanoscale inertial measurement systems with carbon nanotube oscillators *Nanotechnology* **19** 085708

[4] Wang Y Q, Cao L M and Duan X F 2003 Amorphous feather-like boron nanowires *Chem. Phys. Lett.* **367** 495–9

[5] Cao L *et al* 2002 Synthesis of well-aligned boron nanowires and their structural stability under high pressure *J. Phys. Condens. Matter* **14** 11017–21

[6] Xu T T, Zheng J G, Wu N, Nicholls A W, Roth J R, Dikin D A and Ruoff R S 2004 Crystalline boron nanoribbons: synthesis and characterization *Nano Lett.* **4** 5 963–8

[7] Ciuparu D, Klie R F, Zhu Y and Pfefferle L 2004 Synthesis of pure boron single-wall nanotubes *J. Phys. Chem.* B **108** 3967–9

[8] Kiran B, Bulusu S, Zhai H J, Yoo S, Zeng X C and Wang L S 2005 Planar to tubular structural transition in boron clusters: B_{20} as the embryo of single-walled boron nanotubes *PNAS* **102** 961–4

[9] Quandt A, Liu A Y and Boustani I 2001 Density-functional calculations for prototype metal-boron nanotubes *Phys. Rev.* B **64** 125422

[10] Quandt A and Boustani I 2005 Boron nanotubes *Chem. Phys. Chem.* **6** 2001–8

[11] Lau K C, Deshpande M, Pati R and Pandey R 2005 A theoretical study of electronic and vibrational properties of neutral, cationic and anionic B_{24} clusters *Int. J. Quantum Chem.* **103** 866–74

[12] Szwacki N G, Sadrzadeh A and Yakobson B I 2007 B_{80} fullerene: an *ab initio* prediction of geometry stability and electronic structure *Phys. Rev. Lett.* **98** 166804

[13] Boustani I and Quandt A 1998 Boron in ab initio calculations *Comput. Mater. Sci.* **11** 132–7

[14] Boustani I, Quandt A and Rubio A 2000 Boron quasicrystals and boron nanotubes: ab initio study of various B_{96} isomers *J. Solid State Chem.* **154** 269–74

[15] Evans M H, Joannopoulos J D and Pantelides S T 2005 Electronic and mechanical properties of planar and tubular boron structures *Phys. Rev.* B **72** 045434

[16] Tang H and Ismail-Beigi S 2007 Novel precursors for boron nanotubes: the competition of two-center and three-center bonding in boron sheets *Phys. Rev. Lett.* **99** 115501

[17] Wang X, Tian J, Yang T, Bao L, Hui C, Liu F, Shen C, Gu C, Xu N and Gao H 2007 Single crystalline boron nanocones: electric transport and field emission properties *Adv. Mater.* **19** 4480–5

[18] Gindulyte A, Lipscomb W N and Massa L 1998 Proposed boron nanotubes *Inorg. Chem.* **37** 6544–5

[19] Prasad D L V K and Jemmis E D 2006 Boron and MgB_2 analogs of fullerenes and carbon nanotubes: a density functional theory study *J. Mol. Struct. (TheoChem)* **771** 111–5

[20] Kunstmann J and Quandt A 2005 Constricted boron nanotubes *Chem. Phys. Lett.* **402** 21–6

[21] Cabria I, Lopez M J and Alonso J A 2006 Density functional calculations of hydrogen adsorption on boron nanotubes and boron sheets *Nanotechnology* **17** 778–85

[22] Boustani I, Quandt A, Hernandez E and Rubio A 1999 New boron based nanostructured materials *J. Chem. Phys.* **110** 3176–85

[23] Dadashev V, Gindulyte A, Lipscomb W N, Massa L and Squire R 2002 Proposed new materials: boron fullerenes, nanotubes and nanotori *Structures and Mechanisms: from Ashes to enzymes* ed G R Eaton, D C Wiley and O Jardetzky (Washington: Oxford University Press) Chapter 5 pp 79–102

[24] Kunstmann J and Quandt A 2006 Broad boron sheets and boron nanotubes: an *ab initio* study of structural electronic and mechanical properties *Phys. Rev.* B **74** 035413

[25] Cabria I, Alonso J A and Lopez M J 2006 Buckling in boron sheets and nanotubes *Phys. Status Solidi* a **203** 1105–10

[26] Sebetci A, Mete E and Boustani I 2008 Free standing double walled boron nanotubes *J. Phys. Chem. Solids* **69** 2004–12

[27] Yang X, Ding Y and Ni J 2008 *Ab initio* prediction of stable boron sheets and boron nanotubes: structure, stability, and electronic properties *Phys. Rev.* B **77** 041402(R)
[28] Yang X 2008 private communication
[29] Dresselhaus M S, Dresselhaus G and Saito R 1992 Carbon fibers based on C_{60} and their symmetry *Phys. Rev.* B **45** 6234–42
[30] Dresselhaus M S, Dresselhaus G and Saito R 1995 Physics of carbon nanotubes *Carbon* **33** 883–91
[31] Jishi R A, Dresselhaus M S and Dresselhaus G 1993 Symmetry properties of chiral carbon nanotubes *Phys. Rev.* B **47** 16671–4
[32] Cox B J and Hill J M 2007 Exact and approximate geometric parameters for carbon nanotubes incorporating curvature *Carbon* **45** 1453–62
[33] Cox B J and Hill J M 2008 Geometric structure of ultra-small carbon nanotubes *Carbon* **46** 711–3